The Star Formation Newsletter

A community newsletter on Star and Planet Formation research

No. 339 — 21 March 2021
Editor: João Alves www.starformation.news

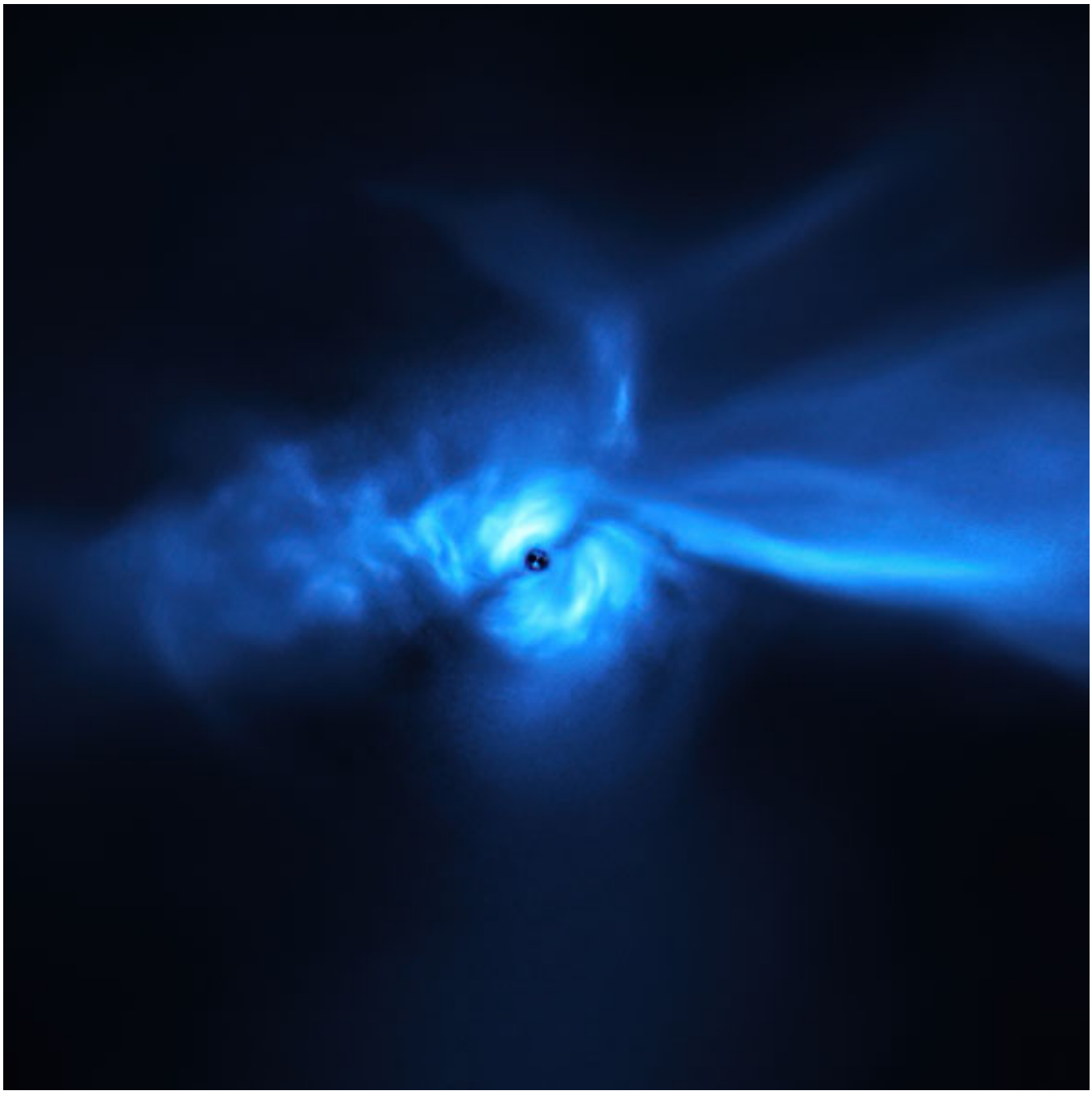

Links to sections

Interviews	Reviews	Perspective	Favorite objects	Archive
Meetings	Jobs	New PhDs	Announcements	Books

Cover image caption

ESO VLT/SPHERE polarimetric observations of the nearby (d ∼ 150 pc) Class II system SU Aur resolving structure down to scales of ∼7 au. The disk shows an intricate spiral structure and a shadow lane, cast by an inner, misaligned disk component. Credit: Ginski et al. 2021, ESO.

Note from the Editor

The Star Formation Newsletter is now on the web at **www.starformation.news**. This PDF file contains the monthly Abstracts and links to the different Newsletter sections. Red text in this PDF is a url link. Submitting an abstract to the SFN is as simple as entering the arXiv ID (e.g., 2006.10139) in a web form on the SFN web site. We extract the title, authors, and the abstract's text directly from the arXiv, so make sure not to remove the LaTeX formatting when submitting to the arXiv. If you do, your abstract will not look great either at the arXiv (which uses MathJax to convert LaTeX math symbols to the web) or the SFN.

Abstracts

1. ## Particle acceleration and magnetic field amplification in massive young stellar object jets

Anabella Araudo, Marco Padovani, Alexandre Marcowith ★ Synchrotron radio emission from non-relativistic jets powered by massive protostars has been reported, indicating the presence of relativistic electrons and magnetic fields of strength ∼0.3-5 mG. We study diffusive shock acceleration and magnetic field amplification in protostellar jets with speeds between 300 and 1500 km/s. We show that the magnetic field in the synchrotron emitter can be amplified by the non-resonant hybrid (Bell) instability excited by the cosmic-ray streaming. By combining the synchrotron data with basic theory of Bell instability we estimate the magnetic field in the synchrotron emitter and the maximum energy of protons. Protons can achieve maximum energies in the range 0.04-0.65 TeV and emit gamma rays in their interaction with matter fields. We predict detectable levels of gamma rays in IRAS 16547-5247 and IRAS 16848-4603. The gamma ray flux can be significantly enhanced by the gas mixing due to Rayleigh-Taylor instability. The detection of this radiation by the Fermi satellite in the GeV domain and the forthcoming Cherenkov Telescope Array at higher energies may open a new window to study the formation of massive stars, as well as diffusive acceleration and magnetic field amplification in shocks with velocities of about 1000 km/s.

2. ## A VLA Census of the Galactic H II Region Population

William P. Armentrout, Loren D. Anderson, Trey V. Wenger, Dana S. Balser, Thomas M. Bania ★ The Milky Way contains thousands of H II region candidates identified by their characteristic mid-infrared morphology, but lacking detections of ionized gas tracers such as radio continuum or radio recombination line emission. These targets thus remain unconfirmed as H II regions. With only ∼2500 confirmed H II regions in the Milky Way, Galactic surveys are deficient by several thousand nebulae when compared to external galaxies with similar star formation rates. Using sensitive 9 GHz radio continuum observations with the Karl G. Jansky Very Large Array (VLA), we explore a sample of H II region candidates in order to set observational limits on the actual total population of Galactic H II regions. We target all infrared-identified "radio quiet" sources from the WISE Catalog of Galactic H II regions between $245^\circ \geq \ell \geq 90^\circ$ with infrared diameters less than $80''$. We detect radio continuum emission from 50% of the targeted H II region candidates, providing strong evidence that most of the radio quiet candidates are bona fide HII regions. We measure the peak and integrated radio flux densities and compare the inferred Lyman continuum fluxes using models of OB-stars. We conclude that stars of approximately spectral type B2 and earlier are able to create H II regions with similar infrared and radio continuum morphologies as the more luminous H II regions created by O-stars. From our 50% detection rate of "radio quiet" sources, we set a lower limit of ∼7000 for the H II region population of the Galaxy. Thus the vast majority of the Milky Way's H II regions remain to be discovered.

3. ALMA-IRDC: Dense gas mass distribution from cloud to core scales

A. T. Barnes, J. D. Henshaw, F. Fontani, J. E. Pineda, G. Cosentino, J. C. Tan, P. Caselli, I. Jiménez-Serra, C. Y. Law, A. Avison, F. Bigiel, S. Feng, S. Kong, S. N. Longmore, L. Moser, R. J. Parker, Á. Sánchez-Monge, K. Wang ★ Infrared dark clouds (IRDCs) are potential hosts of the elusive early phases of high-mass star formation (HMSF). Here we conduct an in-depth analysis of the fragmentation properties of a sample of 10 IRDCs, which have been highlighted as some of the best candidates to study HMSF within the Milky Way. To do so, we have obtained a set of large mosaics covering these IRDCs with ALMA at band 3 (or 3mm). These observations have a high angular resolution (∼3 arcsec or ∼0.05pc), and high continuum and spectral line sensitivity (∼0.15m Jy/beam and ∼0.2K per 0.1km/s channel at the N2H+(1-0) transition). From the dust continuum emission, we identify 96 cores ranging from low- to high-mass (M = 3.4 to 50.9 Msun) that are gravitationally bound and which would require magnetic field strengths of B = 0.3 to 1.0 mG to be in virial equilibrium. We combine these results with a homogenised catalogue of literature cores to recover the hierarchical structure within these clouds over four orders of magnitude in spatial scale (0.01pc to 10pc). Using supplementary observations at an even higher angular resolution, we find that the smallest fragments (< 0.02pc) within this hierarchy do not currently have the mass and/or the density required to form high-mass stars. Nonetheless, the new ALMA observations presented in this paper have facilitated the identification of 19 (6 quiescent and 13 star-forming) cores that retain >16 Msun without further fragmentation. These high-mass cores contain trans-sonic non-thermal motions, are kinematically sub-virial, and require moderate magnetic field strengths for support against collapse. The identification of these potential sites of high-mass star formation represents a key step in allowing us to test the predictions from high-mass star and cluster formation theories.

4. Fragmentation in the massive G31.41+0.31 protocluster

M. T. Beltrán, V. M. Rivilla, R. Cesaroni, L. T. Maud, D. Galli, L. Moscadelli, A. Lorenzani, A. Ahmadi, H. Beuther, T. Csengeri, S. Etoka, C. Goddi, P. D. Klaassen, R. Kuiper, M. S. N. Kumar, T. Peters, Á. Sánchez-Monge, P. Schilke, F. van der Tak, S. Vig, H. Zinnecker ★ Context. ALMA observations at 1.4 mm and 0.2" (750au) angular resolution of the Main core in the high-mass star forming region G31.41+0.31 have revealed a puzzling scenario: on the one hand, the continuum emission looks very homogeneous and the core appears to undergo solid-body rotation, suggesting a monolithic core stabilized by the magnetic field; on the other hand, rotation and infall speed up toward the core center, where two massive embedded free-free continuum sources have been detected, pointing to an unstable core having undergone fragmentation. Aims. To establish whether the Main core is indeed monolithic or its homogeneous appearance is due to a combination of large dust opacity and low angular resolution, we carried out millimeter observations at higher angular resolution and different wavelengths. Methods. We carried out ALMA observations at 1.4 mm and 3.5 mm that achieved angular resolutions of 0.1"(375 au) and 0.075" (280 au), respectively. VLA observations at 7 mm and 1.3 cm at even higher angular resolution, 0.05" (190 au) and 0.07" (260 au), respectively, were also carried out to better study the nature of the free-free continuum sources detected in the core. Results. The millimeter continuum emission of the Main core has been clearly resolved into at least four sources, A, B, C, and D, within 1", indicating that the core is not monolithic. The deconvolved radii of the dust emission of the sources, estimated at 3.5 mm, are 400-500au, their masses range from 15 to 26 Msun, and their number densities are several 1E9 cm-3. Sources A and B, located closer to the center of the core and separated by 750 au, are clearly associated with two free-free continuum sources, likely thermal radio jets, and are the brightest in the core. The spectral energy distribution of these two sources and their masses and sizes are similar and suggest a common origin.

5. Fitting an Analytic Magnetic Field to a Prestellar Core

Gianfranco Bino, Shantanu Basu ★ We deploy and demonstrate the capabilities of the magnetic field model developed by Ewertowski & Basu (2013) by fitting observed polarimetry data of the prestellar core FeSt 1-457. The analytic hourglass magnetic field function derived directly from Maxwell's equations yields a central-to-surface magnetic field strength ratio in the equatorial plane, as well as magnetic field directions with relative magnitudes throughout the core. This fit emerges from a comparison of a single plane of the model with the polarization map that results from the integrated properties of the magnetic field and dust throughout the core. Importantly, our fit is independent of any assumed density profile of the core. We check the robustness of the fit by using the POLARIS code to create synthetic polarization maps that result from the integrated scattering and emission properties of the dust grains and their radiative transfer, employing an observationally-motivated density profile. We find that the synthetic polarization maps obtained from the model also provides a good fit to the observed polarimetry. Our model fits the striking feature of significant curvature of magnetic field lines in the outer part of FeSt 1-457. Combined with independent column density estimates, we infer that the core of size $R_{\rm gas}$ has a mildly supercritical mass-to-flux ratio and may have formed through dynamical motions starting from a significantly larger radius R. A breakdown of flux-freezing through neutral-ion slip (ambipolar diffusion) could be responsible for effecting such a transition from a large-scale magnetic field structure to a more compact gas structure.

6. Self-scattering on large, porous grains in protoplanetary disks with dust settling

Robert Brunngräber, Sebastian Wolf ★ Observations of protoplanetary disks (PPDs) at sub-mm wavelengths suggest that polarisation is caused by scattering of thermal radiation. Most of the dust models that are used to explain these observations have major drawbacks: They either use much smaller grains than expected from dust evolution models, or result in lower polarisations than observed. We investigate the effect of dust grain porosity on the polarisation due to scattering at sub-mm wavelengths arising from grains of up to mm sizes, as they are expected to be present in the midplane of PPDs. Using the effective medium theory, we calculated the optical properties of porous dust and used them to predict the behaviour of the scattering polarisation. Subsequently, radiative transfer simulations for PPDs with porous dust were performed to analyse the additional effect of the optical depth structure, and thus the effect of multiple scattering events and inhomogeneous temperature distributions on the polarisation. We find that porous dust with moderate filling factors of about 10% increase the polarisation compared to compact grains. For higher grain porosities, that is, grains with a filling factor of 1% or lower, the extinction opacity decreases, as does the optical depth of a disk with constant mass. Consequently, the unpolarised direct radiation dominates the scattered flux, and the polarisation drops rapidly. Even though the simulated polarisation is higher than in the case of compact grains, it is still below the typical observed values for face-on disks. However, the polarisation can be increased when crucial model assumptions derived from disk and dust evolution theories, for instance, dust settling and mm-sized dust grains, are dropped. In the case of inclined disks, however, our reference model is able to achieve polarisation degrees of about 1%, and using higher disk masses, even higher than this.

7. Magnetic fields and Star Formation around HII regions: The S235 complex

R. Devaraj, D. P. Clemens, L. K. Dewangan, A. Luna, T. P. Ray, J. Mackey ★ Magnetic fields are ubiquitous and essential in star formation. In particular, their role in regulating formation of stars across diverse environments like HII regions needs to be well understood. In this study, we present magnetic field properties towards the S235 complex using near-infrared (NIR) H-band polarimetric observations, obtained with the Mimir and POLICAN instruments. We selected 375 background stars in the field through combination of Gaia distances and extinctions from NIR colors. The plane-of-sky (POS) magnetic field orientations inferred from starlight polarization angles reveal a curved morphology tracing the spherical shell of the HII region. The large-scale magnetic field traced by Planck is parallel to the Galactic plane. We identified 11 dense clumps using 1.1 mm dust emission, with masses between $33 - 525\,M_{\odot}$. The clump averaged POS magnetic field strengths were estimated to be between $36 - 121\,\mu$G, with a mean of $\sim$65 μG. The mass-to-flux ratios for the clumps are found to be sub-critical with turbulent Alfvén Mach numbers less than 1, indicating a strongly magnetized region. The clumps show scaling of magnetic field strength vs density with a power-law index of 0.52 ± 0.07, similar to ambipolar diffusion models. Our results indicate the S235 complex is a region where stellar feedback triggers new stars and the magnetic fields regulate the rate of new star formation.

8. Water in star-forming regions (WISH): Physics and chemistry from clouds to disks as probed by Herschel spectroscopy

E. F. van Dishoeck, L. E. Kristensen, the WISH team ★ (abridged) Data and results from the WISH key program are summarized, designed to provide a legacy data set to address its physics and chemistry. WISH targeted ~80 sources along the two axes of luminosity and evolutionary stage: from low- to high-mass protostars and from pre-stellar cores to protoplanetary disks. Lines of H2O, HDO, OH, CO and [O I] were observed with the HIFI and PACS instruments, complemented by molecules that probe UV, X-ray or grain chemistry. Most of the far-infrared water emission from protostars is found to be compact, originating from warm outflowing and shocked gas at high density and temperature in at least two physical components. This gas is not probed by low-J CO lines, only by J>14. Water is a significant, but not dominant, coolant. Its abundance is universally low, of order H2O/H2=2E-6, pointing to shock and outflow cavity models that include UV radiation at 100-1000 times the ISRF. In cold quiescent pre-stellar cores and envelopes, the water abundance structure is accurately probed through velocity-resolved line profiles, confirming basic chemistry networks. The gaseous HDO/H2O ratio of 0.025, much higher than that of bulk ice, is representative of the outer photodesorbed ice layers and cold chemistry. Water abundances in the inner hot cores are high, but with variations from 5E-6 to 2E-4. Combined analyses of water gas and ice show that up to 50possible explanations discussed. Water vapor emission from disks is weak, indicating that water ice is locked up in larger pebbles early on and that these pebbles have settled and drifted inward by the Class II stage. Quantitatively, many oceans of water ice are available. Extragalactic low-J H2O emission is mostly compact and collisionally excited. Prospects for future mid- to far-infrared missions are given.

9. Astrochemistry associated with planet formation

Ewine F. van Dishoeck, Edwin A. Bergin ★ This paper provides a brief summary and overview of the astrochemistry associated with the formation of stars and planets. It is aimed at new researchers in the field to enable them to obtain a quick overview of the landscape and key literature in this rapidly evolving area. The journey of molecules from clouds to protostellar envelopes, disks and ultimately exoplanet atmospheres is described. The importance of the close relation between the chemistry of gas and ice and the physical structure and evolution of planet-forming disks, including the growth and drift of grains and

the locking up of elements at dust traps, is stressed. Using elemental abundance ratios like C/O, C/N, O/H in exoplanetary atmospheres to link them to their formation sites is therefore not straightforward. Interesting clues come from meteorites and comets in our own solar system, as well as from the composition of Earth. A new frontier is the analysis of the kinematics of molecular lines to detect young planets in disks. A number of major questions to be addressed in the coming years are formulated, and challenges and opportunities are highlighted.

10. Testing the models of X-ray driven photoevaporation with accreting stars in the Orion Nebula Cluster

Stefan Flaischlen, Thomas Preibisch, Carlo Felice Manara, Barbara Ercolano ★ Recent works highlight the importance of stellar X-rays on the evolution of the circumstellar disks of young stellar objects, especially for disk photoevaporation. A signature of this process may be seen in the so far tentatively observed dependence of stellar accretion rates on X-ray luminosities. According to models of X-ray driven photoevaporation, stars with higher X-ray luminosities should show lower accretion rates, on average, in a sample with similar masses and ages. To this aim, we have analyzed X-ray properties of young stars in the Orion Nebula Cluster determined with Chandra during the COUP observation as well as accretion data obtained from the photometric catalog of the HST Treasury Program. With these data, we have performed a statistical analysis of the relation between X-ray activity and accretion rates using partial linear regression analysis. The initial anticorrelation found with a sample of 332 young stars is considerably weaker compared to previous studies. However, excluding flaring activity or limiting the X-ray luminosity to the soft band (0.5 - 2.0 keV) leads to a stronger anticorrelation, which is statistically more significant. Furthermore, we have found a weak positive correlation between the higher component of the plasma temperature gained in the X-ray spectral fitting and the accretion rates, indicating that the hardness of the X-ray spectra may influence the accretion process. There is evidence for a weak anticorrelation, as predicted by theoretical models, suggesting that X-ray photoevaporation modulates the accretion rate through the inner disk at late stages of disk evolution, leading to a phase of photoevaporation-starved accretion.

11. The Anatomy of an Unusual Edge-on Protoplanetary Disk. II. Gas temperature and a warm outer region

Christian Flores, Gaspard Duchene, Schuyler Wolff, Marion Villenave, Karl Stapelfeldt, Jonathan P. Williams, Christophe Pinte, Deborah Padgett, Michael S. Connelley, Gerrit van der Plas, Francois Menard, Marshall D. Perrin ★ We present high-resolution ^{12}CO and ^{13}CO 2-1 ALMA observations, as well as optical and near-infrared spectroscopy, of the highly-inclined protoplanetary disk around SSTC2D J163131.2-242627. The spectral type we derive for the source is consistent with a 1.2 $M_\odot$ star inferred from the ALMA observations. Despite its massive circumstellar disk, we find little to no evidence for ongoing accretion on the star. The CO maps reveal a disk that is unusually compact along the vertical direction, consistent with its appearance in scattered light images. The gas disk extends about twice as far away as both the submillimeter continuum and the optical scattered light. CO is detected from two surface layers separated by a midplane region in which CO emission is suppressed, as expected from freeze-out in the cold midplane. We apply a modified version of the Topographically Reconstructed Distribution method presented by Dutrey et al. 2017 to derive the temperature structure of the disk. We find a temperature in the CO-emitting layers and the midplane of $\sim$33 K and $\sim$20 K at R $<$ 200 au, respectively. Outside of R $>$ 200 au, the disk's midplane temperature increases to $\sim$30 K, with a nearly vertically isothermal profile. The transition in CO temperature coincides with a dramatic reduction in the sub-micron and sub-millimeter emission from the disk. We interpret this as interstellar UV radiation providing an additional source of heating to the outer part of the disk.

12. Physical and Chemical Structure of the Disk and Envelope of the Class 0/I Protostar L1527

Lizxandra Flores-Rivera, Susan Terebey, Karen Willacy, Andrea Isella, Neal Turner, Mario Flock ★ Sub-millimeter spectral line and continuum emission from the protoplanetary disks and envelopes of protostars are powerful probes of their structure, chemistry, and dynamics. Here we present a benchmark study of our modeling code, RadChemT, that for the first time uses a chemical model to reproduce ALMA $C^{18}O$ (2-1) and CARMA ^{12}CO (1-0) and N_2H^+ (1-0) observations of L1527, that allow us to distinguish the disk, the infalling envelope and outflow of this Class 0/I protostar. RadChemT combines dynamics, radiative transfer, gas chemistry and gas-grain reactions to generate models which can be directly compared with observations for individual protostars. Rather than individually fit abundances to a large number of free parameters, we aim to best match the spectral line maps by (i) adopting a physical model based on density structure and luminosity derived primarily from previous work that fit SED and 2D imaging data, updating it to include a narrow jet detected in CARMA and ALMA data near ($\leq$ 75au) the protostar, and then (ii) computing the resulting astrochemical abundances for 292 chemical species. Our model reproduces the $C^{18}O$ and N_2H^+ line strengths within a factor of 3.0; this is encouraging considering the pronounced abundance variation (factor $> 10^3$) between the outflow shell and CO snowline region near the midplane. Further, our modeling confirms suggestions regarding the anti-correlation between N_2H^+ and the CO snowline between 400 au to 2,000 au from the central star. Our modeling tools represent a new and powerful capability with which to exploit the richness of spectral line

imaging provided by modern submillimeter interferometers.

13. ALMA-IRDC II. First high-angular resolution measurements of the 14N/15N ratio in a large sample of infrared-dark cloud cores

F. Fontani, A. T. Barnes, P. Caselli, J. D. Henshaw, G. Cosentino, I. Jiménez-Serra, J. C. Tan, J. E. Pineda, C. Y. Law ★ The 14N/15N ratio in molecules exhibits a large variation in star-forming regions, especially when measured from N2H+ isotopologues. However, there are only a few studies performed at high-angular resolution. We present the first interferometric survey of the 14N/15N ratio in N2H+ obtained with the Atacama Large Millimeter Array towards four infrared-dark clouds harbouring 3 mm continuum cores associated with different physical properties. We detect N15NH+ (1-0) in about 20-40values measured towards the millimeter continuum cores range from a minimum of 80 up to a maximum of 400. The spread of values is narrower than that found in any previous single-dish survey of high-mass star-forming regions, and than that obtained using the total power data only. This suggests that the 14N/15N ratio is on average higher in the diffuse gaseous envelope of the cores, and stresses the need for high-angular resolution maps to measure correctly the 14N/15N ratio in dense cores embedded in IRDCs. The average 14N/15N ratio of 210 is also lower than the interstellar value at the Galactocentric distance of the clouds (300-330), although the sensitivity of our observations does not allow us to unveil 14N/15N ratios higher than 400. No clear trend is found between the 14N/15N ratio and the core physical properties. We find only a tentative positive trend between 14N/15N and the H2 column density. However, firmer conclusions can be drawn only with higher sensitivity measurements.

14. Disk Evolution Study Through Imaging of Nearby Young Stars (DESTINYS): Late infall causing disk misalignment and dynamic structures in SU Aur

C. Ginski, S. Facchini, J. Huang, M. Benisty, D. Vaendel, L. Stapper, C. Dominik, J. Bae, F. Menard, G. Muro-Arena, M. Hogerheijde, M. McClure, R. G. van Holstein, T. Birnstiel, Y. Boehler, A. Bohn, M. Flock, E. E. Mamajek, C. F. Manara, P. Pinilla, C. Pinte, A. Ribas ★ Gas-rich circumstellar disks are the cradles of planet formation. As such, their evolution will strongly influence the resulting planet population. In the ESO DESTINYS large program, we study these disks within the first 10 Myr of their development with near-infrared scattered light imaging. Here we present VLT/SPHERE polarimetric observations of the nearby class II system SU Aur in which we resolve the disk down to scales of ∼7 au. In addition to the new SPHERE observations, we utilize VLT/NACO, HST/STIS and ALMA archival data. The new SPHERE data show the disk around SU Aur and extended dust structures in unprecedented detail. We resolve several dust tails connected to the Keplerian disk. By comparison with ALMA data, we show that these dust tails represent material falling onto the disk. The disk itself shows an intricate spiral structure and a shadow lane, cast by an inner, misaligned disk component. Our observations suggest that SU Aur is undergoing late infall of material, which can explain the observed disk structures. SU Aur is the clearest observational example of this mechanism at work and demonstrates that late accretion events can still occur in the class II phase, thereby significantly affecting the evolution of circumstellar disks. Constraining the frequency of such events with additional observations will help determine whether this process is responsible for the spin-orbit misalignment in evolved exoplanet systems.

15. K-band High-Resolution Spectroscopy of Embedded Massive Protostars

Tien-Hao Hsieh, Michihiro Takami, Michael S. Connelley, Sheng-Yuan Liu, Yu-Nung Su, Naomi Hirano, Motohide Tamura, Masaaki Otsuka, Jennifer L. Karr, Tae-Soo Pyo ★ A classical paradox in high-mass star formation is that powerful radiation pressure can halt accretion, preventing further growth of a central star. Disk accretion has been proposed to solve this problem, but the disks and the accretion process in high-mass star formation are poorly understood. We executed high-resolution (R=35,000-70,000) iSHELL spectroscopy in K-band for eleven high-mass protostars. Br-γ emission was observed toward eight sources, and the line profiles for most of these sources are similar to those of low-mass PMS stars. Using an empirical relationship between the Br-γ and accretion luminosities, we tentatively estimate disk accretion rates ranging from $\lesssim 10^{-8}$ and $\sim 10^{-4}$ $M_\odot$ yr^{-1}. These low-mass-accretion rates suggest that high-mass protostars gain more mass via episodic accretion as proposed for low-mass protostars. Given the detection limits, CO overtone emission (v=2-0 and 3-1), likely associated with the inner disk region ($r \ll 100$ au), was found towards two sources. This low-detection rate compared with Br-γ emission is consistent with previous observations. Ten out of the eleven sources show absorption at the v=0-2 R(7) − R(14) CO R-branch. Most of them are either blueshifted or redshifted, indicating that the absorption is associated with an outflow or an inflow with a velocity of up to $\sim$ 50 km s^{-1}. Our analysis indicates that the absorption layer is well thermalized (and therefore $n_{\rm H_2} \gtrsim 10^6$ cm^{-3}) at a single temperature of typically 100-200 K, and located within 200-600 au of the star.

16. A pebble accretion model for the formation of the terrestrial planets in the Solar System

Anders Johansen, Thomas Ronnet, Martin Bizzarro, Martin Schiller, Michiel Lambrechts, Åke Nordlund, Helmut Lammer ★ Pebbles of millimeter sizes are abundant in protoplanetary discs around young stars. Chondrules inside

primitive meteorites - formed by melting of dust aggregate pebbles or in impacts between planetesimals - have similar sizes. The role of pebble accretion for terrestrial planet formation is nevertheless unclear. Here we present a model where inwards-drifting pebbles feed the growth of terrestrial planets. The masses and orbits of Venus, Earth, Theia (which later collided with the Earth to form the Moon) and Mars are all consistent with pebble accretion onto protoplanets that formed around Mars' orbit and migrated to their final positions while growing. The isotopic compositions of Earth and Mars are matched qualitatively by accretion of two generations of pebbles, carrying distinct isotopic signatures. Finally, we show that the water and carbon budget of Earth can be delivered by pebbles from the early generation before the gas envelope became hot enough to vaporise volatiles.

17. Magnetohydrostatic Equilibrium Structure and Mass of Polytropic Filamentary Cloud Threaded by Lateral Magnetic Field

Raiga Kashiwagi, Kohji Tomisaka ★ Filamentary structures are recognized as a fundamental component of interstellar molecular clouds in observations by the Herschel satellite. These filaments, especially massive filaments, often extend in a direction perpendicular to the interstellar magnetic field. Furthermore, the filaments sometimes have an apparently negative temperature gradient, that is, their temperature decreases towards the center. In this paper, we study the magnetohydrostatic equilibrium state of negative-indexed polytropic gas with the magnetic field running perpendicular to the axis of the filament. The model is controlled by four parameters: center-to-surface density ratio (ρ_c/ρ_s), plasma β of the surrounding gas, radius of the parent cloud R_0' normalized by the scale height, and the polytropic index N. The steepness of the temperature gradient is represented by N. We found that the envelope of the column density profile becomes shallow when the temperature gradient is large. This reconciles the inconsistency between the observed profiles and those expected from the isothermal models. We compared the maximum line-mass (mass per unit length), above which there is no equilibrium, with that of the isothermal non-magnetized filament. We obtained an empirical formula to express the maximum line-mass of a magnetized polytropic filament as $\lambda_{max} \simeq \left[\left(\lambda_{0,max}(N)/M_\odot \mathrm{pc}^{-1}\right)^2 + (5.0 + 6.0/N)\left(\Phi_{cl}/1\mu\mathrm{G\,pc}\right)^2\right]^{1/2} M_\odot \mathrm{pc}^{-1}$, where $\lambda_{0,max}(N)$ represents the maximum line-mass of the non-magnetized filament and Φ_{cl} indicates one-half of the magnetic flux threading the filament per unit length. Although the negative-indexed polytrope makes the maximum line-mass decrease compared with that of the isothermal model, a magnetic field threading the filament increases the line-mass.

18. ALMA Observations of Giant Molecular Clouds in M33 III: Spatially Resolved Features of the Star-Formation Inactive Million-solar-mass Cloud

Hiroshi Kondo, Kazuki Tokuda, Kazuyuki Muraoka, Atsushi Nishimura, Shinji Fujita, Tomoka Tosaki, Sarolta Zahorecz, Rie E. Miura, Masato I. N. Kobayashi, Sachiko Onodera, Kazufumi Torii, Nario Kuno, Hidetoshi Sano, Toshikazu Onishi, Kazuya Saigo, Yasuo Fukui, Akiko Kawamura, Kisetsu Tsuge, Kengo Tachihara ★ We present ^{12}CO (J = 2-1), ^{13}CO (J = 2-1), and C^{18}O (J = 2-1) observations toward GMC-8, one of the most massive giant molecular clouds (GMCs) in M33 using ALMA with an angular resolution of 0".44 × 0".27 (∼2 pc × 1pc). The earlier studies revealed that its high-mass star formation is inactive in spite of a sufficient molecular reservoir with the total mass of $\sim 10^6$ $M_\odot$. The high-angular resolution data enable us to resolve this peculiar source down to a molecular clump scale. One of the GMC's remarkable features is that a round-shaped gas structure (the "Main cloud") extends over ∼50 pc scale, which is quite different from the other two active star-forming GMCs dominated by remarkable filaments/shells obtained by our series of studies in M33. The fraction of the relatively dense gas traced by the ^{13}CO data with respect to the total molecular mass is only ∼2 structure and the density are not well developed to reach an active star formation. The CO velocity analysis shows that the GMC is composed of a single component as a whole, but we found some local velocity fluctuations in the Main cloud and extra blueshifted components at the outer regions. Comparing the CO with previously published large-scale H I data, we suggest that an external atomic gas flow supplied a sufficient amount of material to grow the GMC up to $\sim 10^6$ $M_\odot$.

19. High-resolution CARMA Observation of Molecular Gas in the North America and Pelican Nebulae

Shuo Kong, Héctor G. Arce, John M. Carpenter, John Bally, Volker Ossenkopf-Okada, Álvaro Sánchez-Monge, Anneila I. Sargent, Sümeyye Suri, Peregrine McGehee, Dariusz C. Lis, Ralf Klessen, Steve Mairs, Catherine Zucker, Rowan J. Smith, Fumitaka Nakamura, Thushara G. S. Pillai, Jens Kauffmann, Shaobo Zhang ★ We present the first results from a CARMA high-resolution ^{12}CO(1-0), ^{13}CO(1-0), and C^{18}O(1-0) molecular line survey of the North America and Pelican (NAP) Nebulae. CARMA observations have been combined with single-dish data from the Purple Mountain 13.7m telescope to add short spacings and produce high-dynamic-range images. We find that the molecular gas is predominantly shaped by the W80 HII bubble that is driven by an O star. Several bright rims are probably remnant molecular clouds heated and stripped by the massive star. Matching these rims in molecular lines and optical images, we construct a model of the three-dimensional structure of the NAP complex. Two groups of molecular clumps/filaments are on the near side of the bubble, one being pushed toward us, whereas the other is moving toward the bubble. Another group is on the far side

of the bubble and moving away. The young stellar objects in the Gulf region reside in three different clusters, each hosted by a cloud from one of the three molecular clump groups. Although all gas content in the NAP is impacted by feedback from the central O star, some regions show no signs of star formation, while other areas clearly exhibit star formation activity. Other molecular gas being carved by feedback includes the cometary structures in the Pelican Head region and the boomerang features at the boundary of the Gulf region. The results show that the NAP complex is an ideal place for the study of feedback effects on star formation.

20. Evidence of Core Growth in the Dragon Infrared Dark Cloud: A Path for Massive Star Formation

Shuo Kong, Héctor G. Arce, Yancy Shirley, Colton Glasgow ★ A sample of 1.3 mm continuum cores in the Dragon infrared dark cloud (also known as G28.37+0.07 or G28.34+0.06) is analyzed statistically. Based on their association with molecular outflows, the sample is divided into protostellar and starless cores. Statistical tests suggest that the protostellar cores are more massive than the starless cores, even after temperature and opacity biases are accounted for. We suggest that the mass difference indicates core mass growth since their formation. The mass growth implies that massive star formation may not have to start with massive prestellar cores, depending on the core mass growth rate. Its impact on the relation between core mass function and stellar initial mass function is to be further explored.

21. SPICY: The Spitzer/IRAC Candidate YSO Catalog for the Inner Galactic Midplane

Michael A. Kuhn, Rafael S. de Souza, Alberto Krone-Martins, Alfred Castro-Ginard, Emille E. O. Ishida, Matthew S. Povich, Lynne A. Hillenbrand ★ We present ∼120,000 Spitzer/IRAC candidate young stellar objects (YSOs) based on surveys of the Galactic midplane between l 255 deg and 110 deg, including the GLIMPSE I, II, and 3D, Vela-Carina, Cygnus X, and SMOG surveys (613 square degrees), augmented by near-infrared catalogs. We employed a classification scheme that uses the flexibility of a tailored statistical learning method and curated YSO datasets to take full advantage of IRAC's spatial resolution and sensitivity in the mid-infrared ∼3-9 micron range. Multi-wavelength color/magnitude distributions provide intuition about how the classifier separates YSOs from other red IRAC sources and validate that the sample is consistent with expectations for disk/envelope-bearing pre-main-sequence stars. We also identify areas of IRAC color space associated with objects with strong silicate absorption or polycyclic aromatic hydrocarbon emission. Spatial distributions and variability properties help corroborate the youthful nature of our sample. Most of the candidates are in regions with mid-IR nebulosity, associated with star-forming clouds, but others appear distributed in the field. Using Gaia DR2 distance estimates, we find groups of YSO candidates associated with the Local Arm, the Sagittarius-Carina Arm, and the Scutum-Centaurus Arm. Candidate YSOs visible to the Zwicky Transient Facility tend to exhibit higher variability amplitudes than randomly selected field stars of the same magnitude, with many high-amplitude variables having light-curve morphologies characteristic of YSOs. Given that no current or planned instruments will significantly exceed IRAC's spatial resolution while possessing its wide-area mapping capabilities, Spitzer-based catalogs such as ours will remain the main resources for mid-infrared YSOs in the Galactic midplane for the near future.

22. Sub-arcsecond Imaging of the Complex Organic Chemistry in Massive Star-forming Region G10.6-0.4

Charles J. Law, Qizhou Zhang, Karin I. Öberg, Roberto Galván-Madrid, Eric Keto, Hauyu Baobab Liu, Paul T. P. Ho ★ Massive star-forming regions exhibit an extremely rich and diverse chemistry, which in principle provides a wealth of molecular probes, as well as laboratories for interstellar prebiotic chemistry. Since the chemical structure of these sources displays substantial spatial variation among species on small scales ($\lesssim 10^4$ au), high angular resolution observations are needed to connect chemical structures to local environments and inform astrochemical models of massive star formation. To address this, we present ALMA 1.3 mm observations toward OB cluster-forming region G10.6-0.4 (hereafter "G10.6") at a resolution of $0.14''$ (700 au). We find highly-structured emission from complex organic molecules (COMs) throughout the central 20,000 au, including two hot molecular cores and several shells or filaments. We present spatially-resolved rotational temperature and column density maps for a large sample of COMs and warm gas tracers. These maps reveal a range of gas substructure in both O- and N-bearing species. We identify several spatial correlations that can be explained by existing models of COM formation, including NH_2CHO/HNCO and CH_3OCHO/CH_3OCH_3, but also observe unexpected distributions and correlations which suggest that our current understanding of COM formation is far from complete. Importantly, complex chemistry is observed throughout G10.6, rather than being confined to hot cores. The COM composition appears to be different in the cores compared to the more extended structures, which illustrates the importance of high spatial resolution observations of molecular gas in elucidating the physical and chemical processes associated with massive star formation.

23. The old moving groups in the field of Taurus

Jiaming Liu, Min Fang, Hao Tian, Chao Liu, Chengqun Yang, Xiangxiang Xue ★ In this work, we present a systematic search for stellar groups in the Taurus field by applying DBSCAN algorithm to the data from Gaia DR2. We find 22 groups, consisting of 8 young groups (Groups 1-8) at ages of 2-4Myr and distances of ∼130-170pc, 14 old groups (Groups 9-22) at ages of 8-49Myr and distances of ∼110-210pc. We characterize the disk properties of group members and find 19 new disk-bearing stars, 8 of which are in the young groups and 11 others belong to the comparatively old groups at ages of 8-11 Myr. We characterize the accretion properties of the group members with Hα emission line in their LAMOST spectra, and discover one source in Group 10 at an age of 10 Myr which still shows accretion activity. We investigate the kinematic relations among the old groups, and find that Group 9 is kinematically related to the known Taurus members and exclude any kinematic relations between Groups 10-22 and the known Taurus members.

24. A survey of IRAS young stellar object candidates. Searching for large-scale Herbig-Haro objects

Rosario López, Angels Riera, Robert Estalella, Gabriel Gómez ★ Jets and outflows are associated with young stellar objects across the stellar mass spectrum, from brown dwarf protostars to massive, Ae/Be stars. Frequently, the jet morphology is spatially discontinuous because of the temporal variability of the ejection from the driving source. Images covering a wide field of view around the jet driving-source are useful to map the large-scale jet emission and to explore the mass ejection history. The aim of this work was to search for large-scale optical Herbig-Haro (HH) objects lying in a wide field around a sample of IRAS sources, candidates to trace young stellar objects. Deep, narrow-band images through the Hα and [SII] emission lines, and through an off-line continuum filter, covering a wide ($\sim 15'$) field around the IRAS targets were acquired. The images in the three filters were analyzed to identify shock-excited line emission (i.e., HH) in contrast to scattered line emission. New images of a sample of fifteen IRAS sources, obtained in an homogeneous way are presented. HH emission was detected in six fields, and the astrometry of the knot features is given. The nature of the extended emission as scattered emission around nine of the IRAS targets is confirmed. For seven IRAS sources, with unclear optical counterpart, a more plausible counterpart is proposed. A refined value of the source distance is reported for seven targets. An update of the main data available for each of the sampled fields, including images from public data archives, is also presented.

25. Molecular Clouds in the Second Quadrant of the Milky Way Mid-plane from l=104.°75 to l=119.°75 and b=−5.°25 to b=5.°25

Yuehui Ma, Hongchi Wang, Chong Li, Lianghao Lin, Yan Sun, Ji Yang ★ We have studied the properties of molecular clouds in the second quadrant of the Milky Way Mid-plane from l=104.°75 to l=119.°75 and b= −5.°25 to b=5.°25 using the ^{12}CO, ^{13}CO, and C^{18}O $J = 1-0$ emission line data from the Milky Way Imaging Scroll Painting project (MWISP). We have identified 857 and 300 clouds in the ^{12}CO and ^{13}CO spectral cubes, respectively, using the DENDROGRAM + SCIMES algorithms. The distances of the molecular clouds are estimated and the physical properties like masses, sizes, and surface densities of the clouds are tabulated. The molecular clouds in the Perseus arm are about 30−50 times more massive and 4−6 times larger than the clouds in the Local arm. This result, however, is likely biased by distance selection effects. The surface densities of the clouds are enhanced in the Perseus arm with an average value of ∼100 M$_\odot$ pc^{-2}. We selected the 40 most extended (>0.35 arcdeg^2) molecular clouds from the ^{12}CO catalog to build the H$_2$ column density probability distribution function (N-PDF). About 78% of the N-PDFs of the selected molecular clouds are well fitted with log-normal functions with only small deviations at high-densities which correspond to star-forming regions with scales of ∼1-5 pc in the Local arm and ∼5-10 pc in the Perseus arm. About 18% of the selected molecular clouds have power-law N-PDFs at high-densities. In these molecular clouds, the majority of the regions fitted with the power-law correspond to molecular clumps of sizes of ∼1 pc or filaments of widths of ∼1 pc.

26. The Galactic HII Region Luminosity Function at Radio and Infrared Wavelengths

J. L. Mascoop, L. D. Anderson, Trey. V. Wenger, Z. Makai, W. P. Armentrout, Dana. S. Balser, T. M. Bania ★ The Galactic HII region luminosity function (LF) is an important metric for understanding global star formation properties of the Milky Way, but only a few studies have been done and all use relatively small numbers of HII regions. We use a sample of 797 first Galactic quadrant HII regions compiled from the WISE Catalog of Galactic HII Regions to examine the form of the LF at multiple infrared and radio wavelengths. Our sample is statistically complete for all regions powered by single stars of type O9.5V and earlier. We fit the LF at each wavelength with single and double power laws. Averaging the results from all wavelengths, the mean of the best-fit single power law index is $\langle\alpha\rangle = -1.75 \pm 0.01$. The mean best-fit double power law indices are $\langle\alpha_1\rangle = -1.40 \pm 0.03$ and $\langle\alpha_2\rangle = -2.33 \pm 0.04$. We conclude that neither a single nor a double power law is strongly favored over the other. The LFs show some variation when we separate the HII region sample into subsets by heliocentric distance, physical size, Galactocentric radius, and location relative to the spiral arms, but blending individual HII regions into larger complexes does not change the value of the power law indices of the best-fit LF models. The consistency of the power law indices across multiple wavelengths suggests that the LF is independent of wavelength. This implies that infrared and radio

tracers can be employed in place of Hα.

27. Gravitoviscous protoplanetary disks with a dust component. V. The dynamic model for freeze-out and sublimation of volatiles

Tamara Molyarova, Eduard I. Vorobyov, Vitaly Akimkin, Aleksandr Skliarevskii, Dmitri Wiebe, Manuel Güdel
★ The snowlines of various volatile species in protoplanetary disks are associated with abrupt changes in gas composition and dust physical properties. Volatiles may affect dust growth, as they cover grains with icy mantles that can change the fragmentation velocity of the grains. In turn, dust coagulation, fragmentation, and drift through the gas disk can contribute to the redistribution of volatiles between the ice and gas phases. Here we present the hydrodynamic model FEOSAD for protoplanetary disks with two dust populations and volatile dynamics. We compute the spatial distributions of major volatile molecules (H_2O, CO_2, CH_4, and CO) in the gas, on small and grown dust, and analyze the composition of icy mantles over the initial 0.5 Myr of disk evolution. We show that most of ice arrives to the grown dust through coagulation with small grains. Spiral structures and dust rings forming in the disk, as well as photodissociation in the outer regions, lead to the formation of complex snowline shapes and multiple snowlines for each volatile species. During the considered disk evolution, the snowlines shift closer to the star, with their final position being a factor $4-5$ smaller than that at the disk formation epoch. We demonstrate that volatiles tend to collect in the vicinity of their snowlines, both in the ice and gas phases, leading to the formation of thick icy mantles potentially important for dust dynamics. The dust size is affected by a lower fragmentation velocity of bare grains in the model with a higher turbulent viscosity.

28. Dipper-like variability of the Gaia alerted young star V555 Ori

Zsófia Nagy, Elza Szegedi-Elek, Péter Ábrahám, Ágnes Kóspál, Attila Bódi, Jérôme Bouvier, Mária Kun, Attila Moór, Borbála Cseh, Anikó Farkas-Takács, Ottó Hanyecz, Simon Hodgkin, Bernadett Ignácz, Réka Könyves-Tóth, Levente Kriskovics, Gábor Marton, László Mészáros, András Ordasi, András Pál, Paula Sarkis, Krisztián Sárneczky, Ádám Sódor, Zsófia Marianna Szabó, Róbert Szakáts, Dóra Tarczay-Nehéz, Krisztián Vida, Gabriella Zsidi ★ V555 Ori is a T Tauri star, whose 1.5 mag brightening was published as a Gaia science alert in 2017. We carried out optical and near-infrared photometric, and optical spectroscopic observations to understand the light variations. The light curves show that V555 Ori was faint before 2017, entered a high state for about a year, and returned to the faint state by mid-2018. In addition to the long-term flux evolution, quasi-periodic brightness oscillations were also evident, with a period of about 5 days. At optical wavelengths both the long-term and short-term variations exhibited colourless changes, while in the near-infrared they were consistent with changing extinction. We explain the brightness variations as the consequence of changing extinction. The object has a low accretion rate whose variation in itself would not be enough to reproduce the optical flux changes. This behaviour makes V555 Ori similar to the pre-main sequence star AA Tau, where the light changes are interpreted as periodic eclipses of the star by a rotating inner disc warp. The brightness maximum of V555 Ori was a moderately obscured (A_V=2.3 mag) state, while the extinction in the low state was A_V=6.4 mag. We found that while the Gaia alert hinted at an accretion burst, V555 Ori is a standard dipper, similar to the prototype AA Tau. However, unlike in AA Tau, the periodic behaviour was also detectable in the faint phase, implying that the inner disc warp remained stable in both the high and low states of the system.

29. OMC-1 dust polarisation in ALMA Band 7: Diagnosing grain alignment mechanisms in the vicinity of Orion Source I

Kate Pattle, Shih-Ping Lai, Melvyn Wright, Simon Coudé, Richard Plambeck, Thiem Hoang, Ya-Wen Tang, Pierre Bastien, Chakali Eswaraiah, Ray Furuya, Jihye Hwang, Shu-ichiro Inutsuka, Kee-Tae Kim, Florian Kirchschlager, Woojin Kwon, Chang Won Lee, Sheng-Yuan Liu, Aran Lyo, Nagayoshi Ohashi, Mark Rawlings, Mehrnoosh Tahani, Motohide Tamura, Archana Soam, Jia-Wei Wang, Derek Ward-Thompson ★ We present ALMA Band 7 polarisation observations of the OMC-1 region of the Orion molecular cloud. We find that the polarisation pattern observed in the region is likely to have been significantly altered by the radiation field of the $> 10^4$ $L_\odot$ high-mass protostar Orion Source I. In the protostar's optically thick disc, polarisation is likely to arise from dust self-scattering. In material to the south of Source I - previously identified as a region of 'anomalous' polarisation emission - we observe a polarisation geometry concentric around Source I. We demonstrate that Source I's extreme luminosity may be sufficient to make the radiative precession timescale shorter than the Larmor timescale for moderately large grains ($> 0.005-0.1\,\mu$m), causing them to precess around the radiation anisotropy vector (k-RATs) rather than the magnetic field direction (B-RATs). This requires relatively unobscured emission from Source I, supporting the hypothesis that emission in this region arises from the cavity wall of the Source I outflow. This is one of the first times that evidence for k-RAT alignment has been found outside of a protostellar disc or AGB star envelope. Alternatively, the grains may remain aligned by B-RATs and trace gas infall onto the Main Ridge. Elsewhere, we largely find the magnetic field geometry to be radial around the BN/KL explosion centre, consistent with previous observations. However, in the Main Ridge, the magnetic field geometry appears to remain consistent with the larger-scale magnetic field, perhaps indicative of the ability of the dense Ridge to resist disruption by the BN/KL explosion.

30. The substructure of the Perseus star forming region: A survey with Gaia DR2

Tatiana Pavlidou, Aleks Scholz, Paula S. Teixeira ★ We use photometric and kinematic data from Gaia DR2 to explore the structure of the star forming region associated with the molecular cloud of Perseus. Apart from the two well known clusters, IC 348 and NGC 1333, we present five new clustered groups of young stars, which contain between 30 and 300 members, named Autochthe, Alcaeus, Heleus, Electryon and Mestor. We demonstrate these are co-moving groups of young stars, based on how the candidate members are distributed in position, proper motion, parallax and colour-magnitude space. By comparing their colour-magnitude diagrams to isochrones we show that they have ages between 1 and 5 Myr. Using 2MASS and WISE colours we find that the fraction of stars with discs in each group ranges from 10 to 50 percent. The youngest of the new groups is also associated with a reservoir of cold dust, according to the Planck map at 353 GHz. We compare the ages and proper motions of the five new groups to those of IC 348 and NGC 1333. Autochthe is clearly linked with NGC 1333 and may have formed in the same star formation event. The seven groups separate roughly into two sets which share proper motion, parallax and age: Heleus, Electryon, Mestor as the older set, and NGC 1333, Autochthe as the younger set. Alcaeus is kinematically related to the younger set, but at a more advanced age, while the properties of IC 348 overlap with both sets. All older groups in this star forming region are located at higher galactic latitude.

31. Detection of new O-type stars in the obscured stellar cluster Tr 16-SE in the Carina Nebula with KMOS

Thomas Preibisch, Stefan Flaischlen, Christiane Göppl, Barbara Ercolano, Veronica Roccatagliata ★ The Carina Nebula harbors a large population of high-mass stars, including at least 75 O-type and Wolf-Rayet stars, but the current census is not complete since further high-mass stars may be hidden in or behind the dense dark clouds that pervade the association. With the aim of identifying optically obscured O- and early B-type stars in the Carina Nebula, we performed the first infrared spectroscopic study of stars in the optically obscured stellar cluster Tr 16-SE, located behind a dark dust lane south of eta Car. We used the integral-field spectrograph KMOS at the ESO VLT to obtain H- and K-band spectra with a resolution of R sim 4000 (Delta lambda sim 5 A) for 45 out of the 47 possible OB candidate stars in Tr 16-SE, and we derived spectral types for these stars. We find 15 stars in Tr 16-SE with spectral types between O5 and B2 (i.e., high-mass stars with M >= 8 Msun, only two of which were known before. An additional nine stars are classified as (Ae)Be stars (i.e., intermediate-mass pre-main-sequence stars), and most of the remaining targets show clear signatures of being late-type stars and are thus most likely foreground stars or background giants unrelated to the Carina Nebula. Our estimates of the stellar luminosities suggest that nine of the 15 O- and early B-type stars are members of Tr 16-SE, whereas the other six seem to be background objects. Our study increases the number of spectroscopically identified high-mass stars (M >= 8 Msun) in Tr 16-SE from two to nine and shows that Tr 16-SE is one of the larger clusters in the Carina Nebula. Our identification of three new stars with spectral types between O5 and O7 and four new stars with spectral types O9 to B1 significantly increases the number of spectroscopically identified O-type stars in the Carina Nebula.

32. A Galactic survey of radio jets from massive protostars

S. J. D. Purser, S. L. Lumsden, M. G. Hoare, S. Kurtz ★ In conjunction with a previous southern-hemisphere work, we present the largest radio survey of jets from massive protostars to date with high-resolution, ($\sim 0.04''$) VLA observations towards two subsamples of massive star-forming regions of different evolutionary statuses: 48 infrared-bright, massive YSOs and 8 IRDCs containing 16 luminous ($L_{bol} > 10^3\,L_\odot$) cores. For 94% of the MYSO sample we detect thermal radio ($\alpha \geq -0.1$ whereby $S_\nu \propto \nu^\alpha$) sources coincident with the protostar, of which 84% (13 jets and 25 candidates) are jet-like. Radio luminosity is found to scale with L_{bol} similarly to the low-mass case supporting a common mechanism for jet production across all masses. Associated radio lobes tracing shocks are seen towards 52% of jet-like objects and are preferentially detected towards jets of higher radio and bolometric luminosities, resulting from our sensitivity limitations. We find jet mass loss rate scales with bolometric luminosity as $\dot{m}_{jet} \propto {L_{bol}}^{0.9\pm0.2}$, thereby discarding radiative, line-driving mechanisms as the dominant jet-launching process. Calculated momenta show that the majority of jets are mechanically capable of driving the massive, molecular outflow phenomena since $p_{jet} > p_{outflow}$. Finally, from their physical extent we show that the radio emission can not originate from small, optically-thick HII regions. Towards the IRDC cores, we observe increasing incidence rates/radio fluxes with age using the proxy of increasing luminosity-to-mass $\left(\frac{L}{M}\right)$ and decreasing infrared flux ratios $\left(\frac{S_{70\mu m}}{S_{24\mu m}}\right)$. Cores with $\frac{L}{M} < 40\,L_{sol}{M_{sol}}^{-1}$ are not detected above (5.8GHz) radio luminosities of $\sim 1\mathrm{mJy\,kpc}^2$.

33. Complex structure of a proto-brown dwarf

B. Riaz, M. N. Machida ★ We present ALMA ^{12}CO (2-1), ^{13}CO (2-1), C^{18}O (2-1) molecular line observations of a very young proto-brown dwarf system, ISO-OPH 200. We have conducted physical+chemical modelling of the complex internal structure for this system using the core collapse simulations for brown dwarf formation. The model at an age of ∼6000 yr can provide a good fit to the observed kinematics, spectra, and reproduce the complex structures seen in the moment maps. Results from modelling indicate that ^{12}CO emission is tracing an extended (∼1000 au) molecular outflow and a bright shock knot, ^{13}CO

is tracing the outer (∼1000 au) envelope/pseudo-disc, and $C^{18}O$ is tracing the inner (∼500 au) pseudo-disc. The source size of ∼8.6 au measured in the 873μm image is comparable to the inner Keplerian disc size predicted by the model. A 3D model structure of ISO-OPH 200 suggests that this system is viewed partially through a wide outflow cavity resulting in a direct view of the outflow and a partial view of the envelope/pseudo-disc. We have argued that ISO-OPH 200 has been mis-classified as a Class Flat object due to the unusual orientation. The various signatures of this system, notably, the young ∼616 yr outflow dynamical age and high outflow rate ($\sim 1\times10^{-7}$ $M_\odot$ yr^{-1}), silicate absorption in the 10μm mid-infrared spectrum, pristine ISM-like dust in the envelope/disc, comparable sizes of the extended envelope and outflow, indicate that ISO-OPH 200 is an early Class 0 stage system formed in a star-like mechanism via gravitational collapse of a very low-mass core.

34. New Mid-Infrared Imaging Constraints on Companions and Protoplanetary Disks around six Young Stars

D. J. M. Petit dit de la Roche, N. Oberg, M. E. van den Ancker, I. Kamp, R. van Boekel, D. Fedele, V. D. Ivanov, M. Kasper, H. U. Käufl, M. Kissler-Patig, P. A. Miles-Páez, E. Pantin, S. P. Quanz, Ch. Rab, R. Siebenmorgen, L. B. F. M. Waters ★ Mid-infrared imaging traces the sub-micron and micron sized dust grains in protoplanetary disks and it offers constraints on the geometrical properties of the disks and potential companions, particularly if those companions have circumplanetary disks. We use the VISIR instrument and its upgrade NEAR on the VLT to take new mid-infrared images of five (pre-)transition disks and one circumstellar disk with proposed planets and obtain the deepest resolved mid-infrared observations to date in order to put new constraints on the sizes of the emitting regions of the disks and the presence of possible companions. We derotate and stack the data to find the disk properties. Where available we compare the data to ProDiMo (Protoplanetary Disk Model) radiation thermo-chemical models to achieve a deeper understanding of the underlying physical processes within the disks. We apply the circularised PSF subtraction method to find upper limits on the fluxes of possible companions and model companions with circumplanetary disks. We resolve three of the six disks and calculate position angles, inclinations and (upper limits to) sizes of emission regions in the disks, improving upper limits on two of the unresolved disks. In all cases the majority of the mid-IR emission comes from small inner disks or the hot inner rims of outer disks. We refine the existing ProDiMo HD 100546 model SED fit in the mid-IR by increasing the PAH abundance relative to the ISM, adopting coronene as the representative PAH, and increase the outer cavity radius to 22.3 AU. We produce flux estimates for putative planetary-mass companions and circumplanetary disks, ruling out the presence of planetary-mass companions with $L > 0.0028 L_\odot$ for $a > 180$ AU in the HD 100546 system. Upper limits of 0.5 mJy-30 mJy are obtained at 8 μm-12 μm for potential companions in the different disks.

35. Undetected Binary Stars Cause an Observed Mass Dependent Age Gradient in Upper Scorpius

Kendall Sullivan, Adam Kraus ★ Young stellar associations represent a key site for the study of star formation, but to accurately compare observations to models of stellar evolution, the age of an association must be determined. The Upper Scorpius region is the youngest section of the Scorpius-Centaurus OB association, which is the largest collection of nearby, young, low-mass stars. The true age of Upper Scorpius is not clear, and an observed mass-dependent age gradient in Upper Scorpius, as well as in other star-forming regions, complicates age measurements. The age gradient may indicate a genuine astrophysical feature or may be an artifact of unrecognized systematic effects in stellar age measurements. We have conducted a synthetic red-optical low-resolution spectroscopic survey of a simulated analog to the Upper Scorpius star-forming region to investigate the effects of unresolved binary stars (which have mass-dependent demographics) on age measurements of a stellar population. We find that the observed mass-dependent age gradient in Upper Scorpius can be explained by a population of undetected binary stars. For a simulated population with an age of 10 (RMS = 2) Myr, we measure an age of 10.5 (RMS = 3.5) Myr for F stars, and 7.5 (RMS = 5.8) Myr for M stars. This discrepancy is caused by the mass-dependent mass ratio distribution and the variable steepness of the mass-luminosity relation. Our results support the previously suggested 10 Myr age for Upper Scorpius, with a small intrinsic age spread.

36. OH mid-infrared emission as a diagnostic of H_2O UV photodissociation. I. Model and application to the HH 211 shock

Benoît Tabone, Marc C. van Hemert, Ewine F. van Dishoeck, John H. Black ★ Water is an important molecule in interstellar and circumstellar environments. Previous observations of mid-infrared rotational lines of OH suggest that these lines may be used to probe the photodissociation of water. In this work, cross sections for the photodissociation of H_2O resolving the state of the OH fragment are collected and incorporated in a new molecular excitation code called GROSBETA, which includes radiative pumping, collisional (de)excitation, and prompt emission (i.e., following the production of OH in excited states). We find that the OH rotational line intensities in the range 9-16μm, covering rotational transitions with $N_{up} = 18$ to 45, are proportional to the column density of H_2O photodissociated per second by photons in the range 114-143nm and do not depend on other local properties. Provided an independent measurement of the column density of water is available, the strength of the local UV radiation field can be deduced with good accuracy. In contrast, the OH lines at longer far-infrared wavelengths

are primarily produced by IR radiative pumping and collisions. Our model successfully reproduces the OH mid-IR lines in the $10 - 16\mu$m range observed by Spitzer toward the tip of the HH 211 bow-shock and shows that the jet shock irradiates its surroundings, exposing H_2O to a UV photon flux that is about 5×10^3 times larger than the standard interstellar radiation field. We also find that chemical pumping by the reaction $H_2 + O$ may supplement the excitation of lines in the range $16 - 30\mu$m. The mid-infrared lines of OH constitute a powerful diagnostic for inferring the photodissociation rate of water and thus the UV field water is exposed to. Future JWST-MIRI observations will be able to map the photodestruction rate of H_2O in various dense and irradiated environments and provide robust estimates of the local UV radiation field.

37. Carbon Chain Chemistry in Hot-Core Regions around Three Massive Young Stellar Objects Associated with 6.7 GHz Methanol Masers

Kotomi Taniguchi, Eric Herbst, Liton Majumdar, Paola Caselli, Jonathan C. Tan, Zhi-Yun Li, Tomomi Shimoikura, Kazuhito Dobashi, Fumitaka Nakamura, Masao Saito ★ We have carried out observations of CCH ($N = 1-0$), CH_3CN ($J = 5 - 4$), and three ^{13}C isotopologues of HC_3N ($J = 10 - 9$) toward three massive young stellar objects (MYSOs), G12.89+0.49, G16.86–2.16, and G28.28–0.36, with the Nobeyama 45-m radio telescope. Combined with previous results on HC_5N, the column density ratios of $N(CCH)/N(HC_5N)$, hereafter the CCH/HC_5N ratios, in the MYSOs are derived to be $\sim$ 15. This value is lower than that in a low-mass warm carbon chain chemistry (WCCC) source by more than one order of magnitude. We compare the observed CCH/HC_5N ratios with hot-core model calculations (Taniguchi et al. 2019). The observed ratios in the MYSOs can be best reproduced by models when the gas temperature is $\sim$ 85 K, which is higher than in L1527, a low-mass WCCC source ($\sim$ 35 K). These results suggest that carbon-chain molecules detected around the MYSOs exist at least partially in higher temperature regions than those in low-mass WCCC sources. There is no significant difference in column density among the three ^{13}C isotopologues of HC_3N in G12.89+0.49 and G16.86-2.16, while $HCC^{13}CN$ is more abundant than the others in G28.28–0.36. We discuss carbon-chain chemistry around the three MYSOs based on the CCH/HC_5N ratio and the ^{13}C isotopic fractionation of HC_3N.

38. Chemical modeling of the complex organic molecules in the extended region around Sagittarius B2

Yao Wang, Fujun Du, Dmitry Semenov, Hongchi Wang, Juan Li ★ The chemical differentiation of seven COMs in the extended region around Sgr B2 has been observed: CH_2OHCHO, CH_3OCHO, t-HCOOH, C_2H_5OH, and CH_3NH_2 were detected both in the extended region and near the hot cores Sgr B2(N) and Sgr B2(M), while CH_3OCH_3 and C_2H_5CN were only detected near the hot cores. The density and temperature in the extended region are relatively low. Different desorption mechanisms have been proposed to explain the observed COMs in cold regions but fail to explain the deficiency of CH_3OCH_3 and C_2H_5CN. We explored under what physical conditions the chemical simulations can fit the observations and explain the different spatial distribution of these species. We used the Monte Carlo method to perform a detailed parameter space study. We investigated how different mechanisms affect the results. All gas-grain chemical models based on static physics cannot fit the observations. The results based on evolving physical conditions can fit six COMs when $T \sim 30 - 60$ K, but the best-fit temperature is still higher than the observed dust temperature of 20 K. The best agreement at $T \sim 27$ K is achieved by considering a short-duration $\sim 10^2$ yr X-ray burst with $\zeta_{CR} = 1.3 \times 10^{-13}$ s^{-1} when the temperature is 20 K. The reactive desorption is the key mechanism for producing these COMs and inducing the low abundances of CH_3OCH_3 and C_2H_5CN. The evolution of the extended region around Sgr B2 may have begun with a cold, $T \leq 10$ K phase followed by a warm-up phase. When its temperature reached $T \sim 20$ K, an X-ray flare from Sgr A* with a short duration of no more than 100 years was acquired, affecting strongly the Sgr B2 chemistry. The observed COMs retain their observed abundances only several hundred years after such a flare, which could imply that such short-term X-ray flares occur relatively often.

39. The Anatomy of an Unusual Edge-on Protoplanetary Disk I. Dust Settling in a Cold Disk

S. Wolff, G. Duchêne, K. Stapelfeldt, F. Ménard, C. Flores, D. Padgett, C. Pinte, M. Villenave, G. van der Plas, M. Perrin ★ As the earliest stage of planet formation, massive, optically thick, and gas rich protoplanetary disks provide key insights into the physics of star and planet formation. When viewed edge-on, high resolution images offer a unique opportunity to study both the radial and vertical structures of these disks and relate this to vertical settling, radial drift, grain growth, and changes in the midplane temperatures. In this work, we present multi-epoch HST and Keck scattered light images, and an ALMA 1.3 mm continuum map for the remarkably flat edge-on protoplanetary disk SSTC2DJ163131.2-242627, a young solar-type star in ρ Ophiuchus. We model the 0.8 μm and 1.3 mm images in separate MCMC runs to investigate the geometry and dust properties of the disk using the MCFOST radiative transfer code. In scattered light, we are sensitive to the smaller dust grains in the surface layers of the disk, while the sub-millimeter dust continuum observations probe larger grains closer to the disk midplane. An MCMC run combining both datasets using a covariance-based log-likelihood estimation was marginally successful, implying insufficient complexity in our disk model. The disk is well characterized by a flared disk model with an exponentially tapered outer edge viewed nearly edge-on, though some degree of dust settling is required to reproduce

the vertically thin profile and lack of apparent flaring. A colder than expected disk midplane, evidence for dust settling, and residual radial substructures all point to a more complex radial density profile to be probed with future, higher resolution observations.

40. Description of turbulent dynamics in the interstellar medium: multifractal/microcanonical analysis I. Application to Herschel observations of the Musca filament

H. Yahia, N. Schneider, S. Bontemps, L. Bonne, G. Attuel, S. Dib, V. Ossenkopf, A. Turiel, A. Zebadua, D. Elia, S. K. Maji, F. G. Schmitt, J. -F Robitaille ★ Observations of the interstellar medium (ISM) show a complex density and velocity structure which is in part attributed to turbulence. We here present a self-contained introduction to the multifractal formalism in a microcanonical version which allows us for the first time to compute precise turbulence characteristic parameters from a single observational map without the need for averages in a grand ensemble of statistical observables. We focus on studying the 250 mu-m Herschel map of the Musca filament and make use of MHD simulations. We find a clear signature of a multiplicative cascade in Musca with an inertial range from 0.05 to 0.65 pc. We show that the proposed microcanonical approach provides singularity spectra which are truly scale invariant as required to validate any method to analyze multifractality. The obtained, for the first time precise enough, singularity spectrum of Musca is clearly not as symmetric as usually observed in log-normal behavior. We claim that the ISM towards Musca features more a log-Poisson shape of its singularity spectrum. Since log-Poisson behavior is claimed to exist when dissipation is stronger for rare events in turbulent flows in contrast to more homogeneous (in volume and time) dissipation events, we suggest that this deviation from log-normality could trace enhanced dissipation in rare events at small scales, which may explain or is at least consistent with the dominant filamentary structure in Musca. Moreover we find that sub-regions in Musca tends to show different multifractal properties. It strongly suggests that different types of dynamics exist inside the Musca cloud. These differences between sub-regions appear only after eliminating noise features which have the tendency to "log-normalize" an observational map. Our study sets up fundamental tools which will be applied to other galactic clouds and simulations in forthcoming studies.